CLM-P858

CLM-P858

Turbulent correlations and anomalous transport in tokamaks

Part II: Applications to TEXT

A. Thyagaraja
F. A. Haas

UK ATOMIC ENERGY AUTHORITY

Culham Laboratory

CLM-P858

Turbulent correlations and anomalous transport in tokamaks Part II: Applications to TEXT

A. Thyagaraja F. A. Haas

Abstract

A parallel kinetic approach is adopted to explain and interpret recent measurements relating to plasma turbulence and transport in the TEXT tokamak. It is shown that the knowledge of experimentally determined profiles of density, temperature and source strengths combined with measurements of a single fluctuating quantity (e.g. electrostatic potential) can be used to account for energy and particle fluxes and turbulent correlations with other fluctuations (e.g. density) measured in the device. The theory predicts the magnetic fluctuations spectrum which is consistent with the measured density fluctuations. It suggests, independently of the mechanisms responsible for the observed turbulent spectra, that the obseved transport properties are explainable in terms of the electromagnetic turbulence in TEXT. A notable feature of the results is the fact that semi-quantitative agreement with experiment (well within experimental errors in several cases) is secured even though the theoretical model neglects toroidal/trapped particle effects entirely.

General Physics and Theory Division
Culham Laboratory
January 1989

1 INTRODUCTION

This paper is a continuation of Thyagaraja and Haas (1988) which will be referred to hereafter as Part I. The purpose of the present article is to report the results of applying the theoretical approach presented earlier to the TEXT experiments. (Schoch et al (1987), (1988)). A preliminary version of our results using an approximate set of parallel kinetic equations has already been presented (Haas and Thyagaraja (1988)). In the present report, we give the details of much more complete simulations including various consistency checks referred to briefly in Part I. As pointed out there, the aim of this work, unlike many linear turbulence theories, is not only to explain the anomalous χ_e in TEXT, but to give a unified interpretation of all of the experimental data available such as energy and particle fluxes, and the measured fluctuation spectra. As far as we are aware this is the most complete interpretation of the TEXT data to date.

The plan of this paper is as follows: in Section 2 we discuss briefly the conditions obtaining in the TEXT experiment, the nature of the data available and the aim or the simulations. Section 3 contains a brief aide memoire to the reader of the essential results of Part I needed to understand the results. Section 4 presents the detailed results. Section 5 contains a discussion of results and summarises the conclusions. The self-consistency of the solution procedure is discussed in the Appendix.

2 THE TEXT EXPERIMENT AND THE PURPOSE OF THE SIMULATIONS

TEXT is a tokamak operating at the Fusion Research Centre, University of Texas at Austin. It has a major radius of 100cm and a plasma minor radius of 25cm. In this paper, we are concerned with a series of ohmic experiments carried out in TEXT to measure turbulent fluctuation spectra and transport fluxes (Schoch et al (1987), (1988), Ritz et al (1987 a,b) and Wootton (1988)). The toroidal magnetic field for this series of experiments is 2 Tesla. The plasma current of approximately 200 kA corresponds to a limiter q value of 3. The Z_{eff} is estimated to be 1.73. In a series of shots keeping these "external" parameters as constant as possible (along with other controllable sources and sinks), several plasma properties have been measured with a variety of diagnostics. We give below a list of the most important properties measured. The details of the diagnostic equipment and the experimental procedures can be found in the references.

The properties measured correspond in the quasi-steady phases of an ensemble of quasi-identical ohmic discharges. The following mean properties are available: a) electron number

density, $n_o(r)$ (both absolute value and radial profile). b) electron temperature $T_{oe}(r)$. c) ion temperature T_{oi} is available at the magnetic axis, at $r/a = 0.5$ and close to the limiter. d) the particle source $S_o(r)$ has been estimated from H_α measurements and the measured n_o, T_{oe}. e) the ohmic heating power $P_{ohmic}(r)$ and $q_o(r)$ have been estimated from measurements of the poloidal B field. f) the radiated power density $P_{rad}(r)$ has been estimated from bolometric measurements.

From the above measurements, it is possible, using steady-state conservation equations, to estimate, a) the particle flux $\Gamma_{e,i}(r)$; b) the electron (total) heat flux $Q_{\perp e}(r)$; c) the electron-ion (classical) equilibration power $P_{ei}(r)$ (assuming an ion profile $T_{oi}(r)$ consistent with the point measurements); and d) the total ion heat flux $Q_{\perp i}(r)$. Inevitably, the estimates involve considerable experimental uncertainties and it is fair to say that overall, the particle and heat fluxes involve errors comparable with their mean values. The radial variation of the profiles are also subject to experimental error particularly in the saw-tooth ($r/a \lesssim .25$) and the edge ($r/a \leq .9$) regions.

The key new feature of the TEXT series of experiments is the measurement of fluctuation spectra $\frac{\tilde{n}(\underline{r},t)}{n_o}$, $\frac{e\tilde{\phi}(\underline{r},t)}{T_{oe}}$. Thus, the ensemble averaged $r.m.s$ fluctuations $\langle\frac{\tilde{n}^2}{n_o^2}\rangle^{\frac{1}{2}}$ and $\langle\frac{e^2\tilde{\phi}^2}{T_{oe}^2}\rangle^{\frac{1}{2}}$ are available as functions of r/a for $r/a \geq 0.5$. They are measured even in the limiter shadow (i.e. when $r/a > 1$) but we shall not be concerned with this region in our present work. The averages referred to above are supposed to include all the modes (m,n) measurable . The largest m values correspond to $k_\perp \rho_i < 0.3$ where $k_\perp \simeq m/a$ and ρ_i is the ion larmor radius ($\simeq .1cm\, in\, TEXT$). At particular radii information is also available on the spectral content S(k) of the density fluctuations. Frequency spectra have also been obtained (Wootton et al. (1988)). The typical fluctuations are in the drift frequency range from $10 - 150kHz$. The magnetic fluctuation spectrum is not measured in $0 \leq r/a \leq 1$ and little is known about it except conjecture based on probe measurements behind the limiter ($r/a > 1$) where it is known to be rather small in amplitude, unlike the finite-amplitude density and electrostatic potential fluctuations. All the measured fluctuations are known to have (both in amplitude and phase) large (50% or more) experimental errors (c.f. Schoch et al (1988)) . The size of the phase errors have yet to be quantified at the time of writing.

The purpose of the numerical simulations using the parallel kinetic approach developed in Part I can now be stated. We take as data the experimentally measured profiles of $n_o(r), T_{oi,e}(r)$ and $q_o(r)$ (assuming a periodic cylinder geometry with uniform B_{oz} field and circular mean flux surfaces as in Part I). We postulate a spectrum of $\frac{\tilde{B}_r}{B_o}(\underline{r}, b)$ fluctuations with as few free parameter as possible. The methods of Part I enable us to calculate the resultant spectra of $\frac{e\tilde{\phi}}{T_{oe}}$ and $\frac{\tilde{n}}{n_o}$ fluctuations as well as the particle flux $\Gamma(r)$ and the energy

fluxes $Q_{\perp e,i}(r)$. We choose the spectral parameters to match the calculated $\frac{e\tilde{\phi}}{T_{oe}}$ spectrum with the experimentally measured one. It is then found that many of the other experimental spectra and fluxes are reproduced within the error bars. More generally, the principle of energetics simulations such as the present one is to construct a magnetic fluctuation spectrum which (via parallel kinetic theory and the experimental profiles) can account for as many qualitative and quantitative features of the measured spectal correlations and transport fluxes as possible. The postulated magnetic spectrum itself, is of course, a prediction; thus if it is possible to measure experimentally the magnetic fluctuations in the interior of the plasma (ie for $r/a < 1$) a direct test of the theory becomes feasible. In view of the fact that the energetics approach cannot, by itself, predict from first principles a magnetic fluctuation spectrum, it is important to test the hypothesis that there exists at least one such spectrum which can account for all the measured characteristics, at least qualitatively. The answer to this existence problem is by no means obvious or trivial. However, in this paper, we present the formulation and the details of the solution of this problem in the case of TEXT.

3 A SUMMARY OF THE THEORETICAL APPROACH

In this section, we summarize briefly the essential formulae of the theoretical development presented in Part I. Unless explicitly stated otherwise, the notation and conventions are those introduced in Thyagaraja and Haas (1988)(ie Part I). It will be recalled that in the periodic cylinder geometry, R denotes the major radius, and a, the limiter radius. B_{oz} is the (uniform by assumption) mean toroidal field while $B_{o\theta}(r)$ is the mean poloidal field. For the purposes of our simulations, we assume the following: $R = 100cm; a = 25cm; Z_{eff} = 1.73$. The edge (ie limiter value at $r/a = 1$) value of q_o is 3.0 corresponding to a plasma current $I_p = 208kA$. The toroidal field $B_{oz} = 2$ Tesla. For the set of TEXT ohmic discharges modelled, the central electron density $n_o(o) = 4.6 \times 10^{13}/c.c$, $T_{oe}(o) = .83KeV$ whilst $T_{oi}(o) = .65KeV$.

The measured q_o profile is reasonably well-represented by the formula,

$$q_o(r) \equiv 0.8 + 2.2\left(\frac{r}{a}\right)^2 \tag{1}$$

For theoretical calculations, it is also convenient to parametrize the experimental measurements of $T_{oi,e}(r)$ in the form

$$T_{oi,e}(r) \equiv T_{oie}(o) exp\left[-2.25\left(\frac{r}{a}\right)^2\right] \tag{2}$$

and $n_o(r)$ in the form

$$n_o(r) \equiv n_o(o)\, exp[-1.3\left(\frac{r}{a}\right)^2] \tag{3}$$

Figures (1), (2), (3) show that these simple forms provide a reasonable fit to the data points.

The fluctuating electromagnetic fields are represented as follows:

$$\underline{B}(\underline{r},t) \equiv \underline{B}_o(r) + \tilde{\underline{B}}(\underline{r},t) \tag{4}$$

where

$$\underline{B}_o(r) = \hat{e}_z\, B_{oz} + \hat{e}_\theta\, B_{o\theta}(r), \tag{5}$$

$$q_o(r) = \frac{r\, B_{oz}}{R\, B_{o\theta}} \tag{6}$$

$$\tilde{\underline{E}}(\underline{r},t) = \nabla\tilde{\phi} - \frac{1}{c}\frac{\partial \tilde{A}_z}{\partial t}(r,\theta,z,t) \tag{7}$$

$$\tilde{\underline{B}} \equiv \nabla\tilde{A}_z \times \hat{e}_z \tag{8}$$

The fluctuating electrostatic potential $\tilde{\phi}$ and the vector potential $\tilde{A}_z$ are assumed to be periodic functions of θ and $\frac{z}{R}$. The specific choices made for the spectrum of $\tilde{A}_z$ will be discussed in the next section. In the following, it is convenient to use the unit vector $\underline{b}(\underline{r},t)$ defined by,

$$\underline{b}(\underline{r},t) \equiv \frac{\underline{B}}{|\underline{B}|} \equiv \underline{b}_o(r) + \tilde{\underline{b}}(\underline{r},t) \tag{9}$$

It will be assumed throughout that $|\tilde{\underline{b}}| << 1$.

The parallel kinetic approach involves the two distribution functions $f_{e,i}(r,\theta,z,v_{||},t)$ which are periodic in θ and $\frac{z}{R}$. It was shown in Part I that f_e (for example) satisfies the parallel kinetic equation,

$$\begin{aligned}&\frac{\partial fe}{\partial t} + \nabla.\{\left(v_{||}\underline{b} + \underline{v}_{\perp e}(\underline{r},t) + \underline{c}_{\perp e}(\underline{r},v_{||},t)\right) f_e\} \\ &-\frac{e}{m_e}E_{||}\frac{\partial f_e}{\partial v_{||}} = \frac{Df_e}{Dt}|_{coll} + \int S_e\delta(\underline{v}.\underline{b} - v_{||})d\underline{v}\end{aligned} \tag{10}$$

where,

$$\underline{v}_{||e}(\underline{r},t) \equiv \frac{c}{B}(\underline{E} + \frac{\nabla p_e}{en_e}) \times \underline{b} \tag{11}$$

$$\underline{c}_{\perp e}(\underline{r},v_{||},t) \equiv \frac{cT_e}{eB}[\nabla ln(\frac{fe}{ne}) \times \underline{b} + (1 - \frac{v_{||}^2}{v_{the}^2}) \times \underline{d}] \tag{12}$$

$$\underline{d} \equiv (curl\underline{b} \times \underline{b}) \tag{13}$$

$$p_e \equiv m_e \int (v_{||} - \bar{v}_{||e})^2 f_e dv_{||} = m_e v_{the}^2 n_e \tag{14}$$

$$n_e \equiv \int f_e dv_{||} \tag{15}$$

$$T_e \equiv m_e v_{the}^2 \tag{16}$$

$$n_e \bar{v}_{||e} \equiv \int f_e v_{||} dv_{||} \tag{17}$$

$$\frac{Df_e}{Dt} |_{coll} = C'(f_e, f_e) + C'(f_e, f_i) \tag{18}$$

$$\sum_e (\underline{r}, v_{||}, t) \equiv \int S_e \delta(\underline{v}.\underline{b} - v_{||}) d\underline{v} \tag{19}$$

The specific forms for $\sum_e$ do not affect any of the present calculations. The collision operators C' will be specified as required.

The decomposition (9) of $\underline{b}$ into a mean and fluctuating part implies that the variables $f_{e,i}, \Phi$ may be similarly represented:

$$f_{e,i} = f_{o,e,i}(r, v_{||}) + \tilde{f}_{e,i}(\underline{r}, v_{||}, t) \tag{20}$$

$$\Phi = \Phi_o(r) + \tilde{\phi}(\underline{r}, t) \tag{21}$$

assuming the spectrum of $\tilde{\underline{b}}$ to be known, equations are derived from Eq.(10), its ion counterpart and the quasi neutrality relation for the quantities $f_{o,e,i}, \Phi_o, \tilde{f}_{e,i}$ and $\tilde{\phi}$. It is unnecessary to reproduce all the formulae here. It suffices to note that the particle flux $\Gamma(r)$ (shown to be automatically ambipolar) and the energy fluxes $Q_{\perp e,i}(r)$ may be expressed in terms of cross-correlations among the moments of $\tilde{f}_{e,i}$ and $\tilde{b}_r$. General relations are also obtained between $\tilde{b}_r(\underline{r}, t)$ and $\tilde{\phi}(\underline{r}, t), \tilde{n}(\underline{r}, t)$. The key to these relations is the solution of the kinetic equations in powers of the amplitude $\frac{\tilde{B}r}{B_o}$.

4 RESULTS OF THE TEXT SIMULATIONS

4.1 Choice of the assumed magnetic fluctuation spectrum.

As explained in Part I, there is considerable arbitrariness of choice involved in picking a suitable fluctuation spectrum. This is inescapable in a theory of energetics such as ours where the fluctuation spectrum of any one physical property must be taken as given. Heuristic considerations involving both theoretical and experimental inputs are used to reduce the free parameters to a sensible number. Consider $\tilde{b}_r(r, \theta, z, t)$ to be the "primary" fluctuation to be specified. Using the periodicity in θ and $\frac{z}{R}$ we may write quite generally,

$$\tilde{b}_r(r, \theta, z, t) \equiv \sum_{m=-\infty}^{\infty} \sum_{n=-\infty}^{\infty} F_{m,n}(r, t)\, e^{i.(m\theta + \frac{nz}{R})} \tag{22}$$

Firstly, in TEXT it is known that $k_\theta \simeq \frac{m}{a}$ is such that $k_\theta \rho_i \leq 0.3$. We may therefore restrict ourselves to $1 \leq m \leq 50, 1 \leq n \leq 50$. It is technically not feasible to allow an arbitrary time dependence as this involves Stieltjes integrals. We assume therefore that $\tilde{b}_r$ may be written in the form,

$$\tilde{b}_r = \sum_{m=1}^{50} \sum_{n=1}^{50} b_{mn}(r) cos(m\theta - \frac{nz}{R} + \omega_* t) \tag{23}$$

where $\omega_* \equiv \omega_o m$ with $\omega_o = 2000$ rads/sec. This time dependence gives rise to a discrete spectrum with an "effective" frequency ω_* for each m of the order of the drift frequency. The spatial function $b_{mn}(r)$ is totally unknown experimentally. We simply follow earlier work and postulate that it is "localized" about resonant surfaces with radial scale of variation comparable with k_θ. We are therefore led to set,

$$b_{mn}(r) = \epsilon_{mn} \frac{1}{m^{\frac{1}{4}}} \left[\frac{(r/2a)}{(r/a) + 0.1} \right] exp \left\{ -\frac{1}{4}(m - nq_o(r))^2 \right\} \equiv \epsilon_{mn} \Lambda_{mn}(r) \tag{24}$$

In Eq.(24) ϵ_{mn} is a constant amplitude factor which will be discussed further below. The term $m^{-\frac{1}{4}}$ seeks to model the weak fall-off with k_θ of the power spectrum of $\frac{\tilde{n}}{no}$ observed by Ritz et al (1987a). The next term ensures that $b_{mn}(o) = 0$. It also ensures that except within 10% of the magnetic axis, the nominal spatial variation of any m,n mode is given by the resonant exponential factor. There is virtually no information available experimentally on the radial variation of $\tilde{b}_r$ in the confinement and sawtooth zones. The resonant form and the factor $\frac{1}{4}$ were used by us successfully in modeling TFR and JET. (Haas and Thyagaraja (1987)). We have found by extensive trials that whilst this form and others sufficiently "close" to it (in a function-space sense) give the best results for TEXT, it is by no means uniquely fixed by the available experimental data.

Although the experiments of RITZ et al (1987a) have helped to motivate our hypotheses concerning the magnetic fluctuation spectrum, it is important to bear in mind several caveats. Firstly, the experimental measurements strictly refer to the density fluctuation spectra fairly close to the limiter. Referring to FIG. 6a of RITZ et al (1987a), it is clear that for $k_\theta > 2.0$ the power falls off abruptly. This fact is embodied by limiting m to 50 in Eq(23). It is very difficult to determine the exact experimental variation of power with m for $m < 50$. We have tried several choices for the exponent in $(1/m)^\nu$ in Eq.(24) and settled for $\nu = 1/4$ as possibly the best representation over all. As mentioned earlier, other functional forms give equivalent results with more or less the same degree of agreement. Experiment indicates that for each m, n mode the frequency spectrum is a maximum around a frequency ω_* which is proportional to k_θ and is of order the electron drift frequency. Care must be exercised in comparing the signs of the theoretically assumed phase velocities with those seen in

experiment, in view of the fact that the calculations refer to a frame of reference in which the ion fluid is at rest.

It is clear from the above description that the free parameters in $\tilde{b}_r$ have been reduced by virtue of the above hypotheses (some of which derive unchanged from earlier work) to the constants ϵ_{mn} and ω_o. Since we are dealing with 50×50 modes, we have potentially still 2500 free parameters in ϵ_{mn}! These are reduced to just four as follows:

(1) Using the well-known fact from Hamiltonian dynamics of ergodic fields (Moser (1973)), we anticipate that "low-order" resonances can play an important role in the magnetic fluctuation spectrum. We consider only three such "discrete" resonances. Thus, consider all $m, n \leq 50$ such that $m/n = 2$. This collection of (m,n) models will be called the (2,1) family. We assume specifically that for all the members of the family, $\epsilon_{m,n} \equiv \epsilon_{2,1}$, ie the amplitudes are equal. The other two families we include explicitly are (3,1) and (5,2).

(2) The remaining values of (m,n) constitute the "continuum background" (this is just short-hand nomenclature since for any integer m,n, the modes are really discrete. It is less cumbersome than the more accurate "low order" and "high order" spectra). We assume that for any member of the continuum, $\epsilon_{mn} \equiv \epsilon$, where ϵ is a **single** amplitude parameter.

The above assumptions enable us to re-write the spectral representation Eq. (23) as follows.

$$\begin{aligned}
\tilde{b}_(r) \equiv \epsilon \sum_{m=1}^{50}, \sum_{n=1}^{50}, \Lambda_{mn}(r) cos(m\theta - \frac{nz}{R} + \omega_* t) \\
+\epsilon_{2,2} \sum_{m=1}^{50} \sum_{n=1}^{50} \delta_{m,2n} \Lambda_{mn}(r) cos(m\theta - \frac{nz}{R} + \omega_* t) \\
+\epsilon_{5,2} \sum_{m=1}^{50} \sum_{n=1}^{50} \delta_{2m,5n} \Lambda_{mn}(r) cos(m\theta - \frac{nz}{R} + \omega_* t) \\
+\epsilon_{3,1} \sum_{m=1}^{50} \sum_{n=1}^{50} \delta_{m,3n} \Lambda_{mn}(r) cos(m\theta - \frac{nz}{R} + \omega_* t), \qquad (25)
\end{aligned}$$

where δ denotes the usual Kronecker symbol.

We have already stated that $\omega_* \equiv \omega_o m$, $\omega_o = 2000$ rads/sec. It turns out that to represent experiment, the ω_* for the discrete modes must be defined differently. This constitutes the third and final assumption:

$$\omega_*(discretemodes) \equiv \frac{cT_{oi}}{eB_{oz}} \frac{p'_{oi}}{p_{oi}} \frac{m}{r} \qquad (26) .$$

where, the quantities in eq.(26) are evaluated at the resonant point appropriate to the mode in question. In summary, Equations (24),(25),(26) and the specification of the constants $\epsilon, \epsilon_{2,1}, \epsilon_{5,2}, \epsilon_{3,1}$, and ω_o specify $\tilde{b}_r(\underline{r}, t)$ **completely** as a function of position and time if $q_o(r/a), n_o(r/a), T_{oi}(r/a)$ and B_{oz} are known. Since experiment allows the profiles to be readily determined, the only truly free parameters of the theory are $\epsilon, \epsilon_{2,1}, \epsilon_{5,2}, \epsilon_{3,1}$ and ω_o. It is very important to note these are not **functions** but constants. The purpose of the present simulations to show that the parallel kinetic theory developed in Part I together with the spectral assumptions described above are self-consistently able to account for experimentally measured **profiles** (ie functions of r/a) of transport fluxes and relative fluctuations $\frac{\tilde{n}}{n_o}, \frac{e\tilde{\phi}}{T_{oe}}$.

4.2 Comparison of the calculated fluctuating spectra with experiment

We are now in a position to compare theory with experiment. For the reader's convenience, the choices of the parameters used in the numerical simulations are listed in Table I. In Fig. 4a we show plots of the various components of the spectrum assumed for $\tilde{b}_r$. Only the 'continuum' shows a simple radial behaviour. The low (m,n) resonances are easily identified in the three 'discreta'.

Table 1

Toroidal field B_{oz}	=	2 Tesla
Major Radius R	=	100cm
Limiter Radius a	=	25cm
q_o (a)	=	3
Plasma Current I_p	=	208 kAmps
Central electronTemp. $T_{oe}(o)$	=	0.83 KeV
Central ion Temp T_{oi} (o)	=	0.65 KeV
Central electron Density	=	$4.6 \times 10^{13}/c.c$
Z_{eff}	=	1.73
Maximum mode no m_{max}	=	50
ω_o	=	2000 rads/sec
Continuum amplitude ϵ	=	1.2×10^{-4}
(2.1) amplitude $\epsilon_{2,1}$	=	$\epsilon \times 2.5$
(5,2) amplitude $\epsilon_{5,2}$	=	$\epsilon \times 5.0$
(3,1) amplitude $\epsilon_{3,1}$	=	$\epsilon \times 14.0$

In Fig. 4b we show the comparison between the theoretically calculated values of $< \frac{\tilde{n}^2}{n_o^2} >^{\frac{1}{2}}$, $< \left(\frac{e\tilde{\phi}}{T_{oe}}\right)^2 >^{\frac{1}{2}}$ and the experimentally measured ones in the range $0.5 \leq r/a \leq 1$. It should be clearly understood that the choice for $\epsilon = 1.2 \times 10^{-4}$ was governed by requiring the theoretical value for $< \left(\frac{e\tilde{\phi}}{T_{oe}}\right)^2 >^{\frac{1}{2}}$ at $\frac{r}{a} = 0.9$ (the largest value) to equal the experimental one. The choice of $\omega_o, \epsilon_{2,1}, \epsilon_{5,2}, \epsilon_{3,1}$ were more influenced by the agreement overall with the magnitudes of the transport fluxes. Fig. 4b shows that given the experimentally determined profiles of n_o, T_{oe}, T_{oi} and q_o and the assumed $\tilde{b}_r$ spectrum Eq. (25) with the parameters chosen in Table I, the resultant spectra of $\frac{\tilde{n}_e}{n_o}$ and $\frac{e\tilde{\phi}}{T_{oe}}$ reproduce the following features of the experimentally measured spectra.

(i) Given that $< \left(\frac{e\tilde{\phi}}{T_{oe}}\right)^2 >^{\frac{1}{2}}_{theory}$ (r/a=0.9) $= < \left(\frac{e\tilde{\phi}}{T_{oe}}\right)^2 >^{\frac{1}{2}}_{expt}$ (r/a = 0.9) by choice, the theory is able to reproduce the experimental values at other radii qualitatively. The numerical agreement is reasonable given the very large uncertainties in both theory and experiment.

(ii) The size and radial variation of the $\frac{\tilde{n}}{n_o}$ spectrum as measured experimentally is well captured by the theory. The strong non-adiabaticity in intensity apparent in the experimental points (ie. $|\frac{e\tilde{\phi}}{T_{oe}} \neq |\frac{\tilde{n}}{n_o}|$ but generally larger) is seen to be reproduced by the theory. This qualitative fact turns out to be independent of the value of ϵ chosen and depends only on ω_o. It is not very sensitive to the ratios $\epsilon_{2,1}/\epsilon$ etc.

(iii) Experimental values of $\frac{e\tilde{\phi}}{T_{oe}}$ show clearly that the radial variation is not monotonic but some influence of low order resonances exists. This was the motivation in the present study of treating the "continuum" and the "discretum" separately. Qualitative agreement with experiment can be obtained with an "undifferentiated" spectrum in which $\epsilon_{m,n} \equiv \epsilon$ for all m,n and $\omega_{m,n} \equiv m\omega_o$. The explicit treatment of the three most important low order resonances leads to better agreement in the transport fluxes.

4.3 Comparison of the theoretically calculated transport fluxes with experiment

We now turn our attention to the particle and energy fluxes. The particle flux $\Gamma_e(r)$ is calculated by evaluating the expression

$$\Gamma_e(r) \equiv \frac{1}{e} < \tilde{b}_r \tilde{J}_{\|e} > + n_o < v_{\perp er} > + < \tilde{n}\tilde{v}_{\perp er} > \tag{27}$$

where

$$\tilde{J}_{\|e} \equiv -e \int_{-\infty}^{\infty} v_{\|} \tilde{f}_e dv_{\|} \tag{28}$$

A corresponding expression gives $\Gamma_i(r)$. It is an important check on the consistency of the numerical simulations that $\Gamma_e(r) = \Gamma_i(r)$. Indeed, it can be shown that this equality applies to each (m,n) mode **separately**. Having verified its truth, we plot $\Gamma_e(r)$ over the range $0.6 \leq r/a \leq 1$ in Fig.5. For comparison, experimental estimates of the $E \times B$ flux obtained with the heavy ion beam probe and that estimated from the particle source (using $H\alpha$ light diagnostics) are also shown. The experimental diagnostics are available even in the limiter shadow region ($r/a > 1$) where the present theory is inapplicable as it stands. The theoretical values are in reasonable agreement with the particle source measurement. There is qualitative agreement with the HIPB estimates which can have significant amplitude and phase resolution errors associated with the method. Since the fluctuation amplitudes ϵ in Eq(25) was fixed relative to the measurements pf $\frac{e\tilde{\phi}}{T_{oe}}$, the fact that theory and experiment are in reasonable agreement as regards the radial variation and numerical size of $\Gamma_e(r)$ suggests that the assumed magnetic fluctuation spectrum leads to $\frac{\tilde{e}}{n_o}$ and $\frac{e\tilde{\phi}}{T_{oe}}$ spectra which have the right sizes and relative phase to get the correct particle flux.

In Fig.6. we show the experimentally obtained values of $Q_{\perp etot}(r/a)$ (from energy balance taking account of ohmic heating, classical electron-ion equilibration, and radiation) in comparison with the theoretically calculated value (derived from the formula)

$$\begin{aligned} Q_{\perp e}(r) \equiv & < \tilde{b}_r \int_{-\infty}^{\infty} 3\frac{m_e}{2} v_{\|}^3 \tilde{f}_e dv_{\|} > + < v_{\perp er} > \left(3\frac{p_{oe}}{2} + 3\frac{m_e}{2} n_o v_{o\|e}^2 \right) \\ & + \int_{-\infty}^{\infty} 3\frac{m_e}{2} v_{\|}^2 f_{oe} < c_{\perp er} > dv_{\|} \\ & + < \int_{-\infty}^{\infty} \tilde{v}_{\perp e}^{*} 3\frac{m_e}{2} v_{\|}^2 \tilde{f}_e dv_{\|} > \end{aligned} \tag{29}$$

over the range $o \leq r/a \leq 1$.

Except for values within the "inversion radius" where $q_o(r/a) \leq 1$, the calculated values are in good agreement with experiment. There the theoretical calculation appears to overestimate the size of the $q_o = 1$ resonance. This may also be due to the fact that $Q_{\perp cetot}$ (experiment). is not accurate in the sawtooth zone. Thus, the assumed $\tilde{b}_r$ spectrum gives a reasonably good account of the electron energy flux in the confinement and edge zones upto $r/a \lesssim 1$. Better measurements of $\tilde{b}_r$ in the plasma interior would throw further light on the remaining discrepancies.

In the TEXT experiments, the ion temperature T_{oi} is only measured at three locations (at r/a = 0, 0.5 and at the edge). Making certain assumptions, the experimenters have inferred an ion energy flux which we plot in Fig. 7.

The theoretical estimate of the ion heat flux comprises a turbulent (convective energy loss) part given by an expression analogous to Eq.(30) together with a neo-classical part from trapped ions which is not negligible. The total flux is plotted in fig. 7 and compared with

experiment. The calculated values are within the error bars except near r/a = 0.8 (where the (2, 1) island is approximately located) although the experimental estimates are somewhat larger. At present, very little can be said definitely about whether this is a genuine failure of the theory to account for observations or not. More theoretical and experimental work is required before reliable conclusions can be reached.

5 DISCUSSION AND CONCLUSIONS

The results presented in previous sections show that certain general conclusions may be drawn regarding tokamak turbulence and transport. We list them below:

(1) The parallel kinetic approach developed in Part I can be used to calculate turbulent correlations and transport fluxes under tokamak conditions, starting from an assumed magnetic fluctuation spectrum and experimental profiles. We note that the kinetic equations we are using involve both collisions and parallel Landau effects. As such for any assumed fluctuation spectrum of $\tilde{b}_r$ say, the calculation always yields spectra for $e\tilde{\phi}/T_{oe}$ and $\frac{\tilde{n}}{n_o}$, which are related in non-trivial ways in amplitude and phase. It should also be noted that our kinetic equations contain the standard instantaneous collision frequencies which occur in the Boltzmann equation. The aim of the calculation is to obtain the consequences of such a model. It is possible that turbulence by itself alters the collision operators, but in the interests of simplicity we do not consider this possibility.

(2) The quasi-neutrality condition $|\ (n_i - n_e)/n_e\ | << 1$ is implied by $k_\perp \lambda_D << 1$ and $\frac{\omega_*}{\omega_{pe}} << 1$. As shown in Part I, it in turn implies ambipolar particle fluxes. More importantly, it relates magnetic fluctuations to electrostatic fluctuations (ie the $\tilde{b}_r, \frac{e\tilde{\phi}}{T_{oe}}$ relations). This demonstrates that under tokamak conditions, the two effects (electromagnetic and electrostatic) are intimately linked although their relative contributions to the particle and energy fluxes can be different in size.

(3) Low order resonances play an important role in the magnetic fluctuation spectrum in that they appear to be necessary to get quantitative agreement between simulations and experiment.

(4) Purely passing particles colliding classically are clearly able (according to the present simulations) to account for the observed nonadiabaticity in amplitude and phase in the $\frac{\tilde{n}}{n_o}$, $\frac{e\tilde{\phi}}{T_{oe}}$ spectra. As pointed out by Rosenbluth and Rutherford (1981) theoretically, a strong non-adiabaticity, in phase at least, must exist between the above spectra in order

to get significant turbulent particle fluxes. In our model representation of the Stiltjes spectrum, we have used frequencies of order of, but not equal to, the electron drift frequencies at resonance. This failure to be exactly resonant is a characteristic of broad-band turbulence and results in the non-adiabaticity in amplitude and phase shown in Fig. 4b. The agreement with experiment is semi-quantitative. While trapped particles may also play a role, the present simulations suggest that it is not an overwhelmingly important one. Thus at the present level of experimental accuracy and theoretical uncertainty, they can be neglected.

(5) Ion heat fluxes are somewhat larger than would be expected according to neo-classical theory. This observational fact appears to be capable of an unforced turbulence interpretation according to the present model.

(6) No theory such as the present one can give a first-principles explanation of the assumed magnetic fluctuation spectrum. Various linear instability theories involving drift waves, trapped particles etc have been put forward. Whilst linear theory may give useful indications about possible mechanisms, it is wholly wrong as far as leading to a viable method of calculating stationary turbulent states involving 10^4 modes or more over a wide range of frequencies and wave numbers. The so-called renormalization methods are so ad hoc as to defy any sensible physical accounting of the closure hypotheses buried in them. Such methods have also failed badly as far as **practical**, engineering fluid mechanics (or meteorology) are concerned. It would therefore appear that further progress is only possible by much more systematic experimental measurements of spectra and fluxes (in particular magnetic fluctuations in the **interior** of the plasma $0 \leq r/a \leq .8$). TEXT's pioneering diagnostics could be used in other ways (for example, the present theory can also estimate trace impurity transport under the conditions of the above simulations using the **same** assumed spectrum) to remove uncertainties. Future theoretical effort will be devoted to the possibility of nonlinearly solving the full set of parallel kinetic equations, Ampere's law and quasi-neutrality condition to determine the nature of the spectrum for at least the lower values of m,n ($1 \leq m \leq 20$ say). Such a simulation would, at the very least, provide further guidance in the construction of practically useful spectral models and scaling relations.

It is important to recognize that a small amplitude turbulence theory must be nonlinear if a spectrum is to be calculated. The spectrum of turbulence is always the result of nonlinear interactions leading to statistically stationary states; although linear instabilities may be (this is not a necessary condition, as shown by pipe flow) involved in the transition to turbu-

lence, they are not useful in describing fully developed turbulence such as that observed in tokamaks. The situation is analogous to the Stokes theory of water waves (Whitham (1975)) where the smallness of the amplitude is used but the theory gives a nonlinear dispersion relation. In a future work we hope to address ourselves to the generalization of parallel kinetic theory needed for generating the spectrum from theoretical first principles.

Acknowledgement

The authors express their thanks to Dr. A. J. Wootton and the TEXT team members who discussed their experimental data with them, in many cases in advance of publication. They are very grateful to Mrs Gladys Lane for her careful preparation of this paper. They also wish to thank the referees for their stimulating comments.

References

HAAS F.A. and THYAGARAJA A. (1987) *Plasma Physics and Controlled Fusion*, **29**, p145.

HAAS F.A. and THYAGARAJA A. (1988) *Proc. 15th Euro. Conf. on Controlled Fusion and Plasma Heating, (Dubrovnic)*, Vol I, p.270.

MOSER J. (1973) **Stable and Random motions in Dynamical Systems**, Princeton Univ. Press, Princeton, N.J.

RITZ Ch.P. et al. (1987a) *Nuclear Fusion*, **27**, No. 7, 1125.

RITZ Ch.P. et al. (1987b) *Journal of Nuclear Mats.*. 145-147, p241.

ROSENBLUTH, M.N. and RUTHERFORD, P.H. (1981), Chapter II in *Fusion* 1, 31, ed. E.Teller (Academic Press, London).

SCHOCH P.M., et al. (1987) *Proc. 14th Euro. Conf. on Controlled Fusion and Plasma Physics, (Madrid)*, **1**, p126.

SCHOCH P.M., et al. (1988), *FRC Report.#* 312.

THYAGARAJA A. and HAAS F.A. (1988) *Culham Laboratory Report* CLM - P 846. (Accepted for publication in Plasma Physics and Controlled Fusion).

WHITHAM G.B. (1974) **Linear and Nonlinear Waves** Wiley, New York.

WOOTTON A.J. et al (1988) *Plasma Physics and Controlled Fusion* , **30**, p1479.

Appendix

Consistency Checks on the Numerical Simulations

Given the analytical and numerical complexity of the simulations outlined in Part I and implemented for TEXT conditions in the present report, it is important to have internal consistency checks performed for the typical conditions. We briefly describe a set of such checks and present the results.

It was shown in Part I that whatever the spectrum chosen, $\Gamma_i(r)$ must always equal $\Gamma_e(r)$ although quite different correlations are involved in calculating these quantities. It is therefore a measure of consistency to calculate the relative error $\left|\frac{\Gamma_i(r)-\Gamma_e(r)}{\Gamma_e(r)}\right|$ where these fluxes are estimated numerically using the analytic formulæ given in Part I. It should be apparent that in this case, the checks can be made both for a single (m,n) mode (i.e including only a single term from Eq. (25)) or for the entire spectrum. In either case, the result is that the maximum relative error is less than 0.1% . Thus, the code always (irrespective of the spectrum) leads to ambipolar particle fluxes in conformity with the general result of Part I.

The second set of checks concerns the fluctuating $\tilde{f}_{e,i}$. The reader will doubtless recall that for each (m,n,ω) mode, these were obtained in terms of the velocity space functions $\overline{X}_{e,i}$ etc and their own velocity moments $\tilde{n}_{i,e}, \tilde{v}_{\|i,e}, \tilde{p}_{i,e}$. An obvious and elementary check on the velocity space solutions $\overline{X}_{e,i}(x)$ is to take the moments of $\tilde{f}_{e,i}$ **after** the solution and compare them with those obtained directly. When performed, it turns out that the post solution moments agree with the solved moments to the accuracy with which the velocity space integrals are evaluated ($ie \lesssim 1\%$).

For the given, (m,n,ω) mode, a third set of checks on the moments $\tilde{n}, \tilde{v}_{\|e,i}, \tilde{p}_{e,i}$ may be obtained by substituting them in the electron and ion continuity equations and the two parallel momentum equations. Note that the energy equations involve higher moments and hence cannot be thus checked for consistency. With suitable non-dimensional definitions of relative error, we find that the moments obtained from the solution procedure (this does not explicitly involve solving the corresponding moment equations) satisfy the respective moment equations to very high accuracy (typically $\epsilon \simeq 10^{-3}$) except possibly at $r = o, a$ or the resonant radius of the mode, where the relative error is of the order of 1%.

Finally, we have checked that both the BGK collision operators (used in the text) and the Fokker-Planck operators give the same results to the calculated accuracy. We conclude that the parallel-kinetic equations formulated in Part I are being correctly solved by our numerical code and the resultant solutions satisfy the above consistency checks.

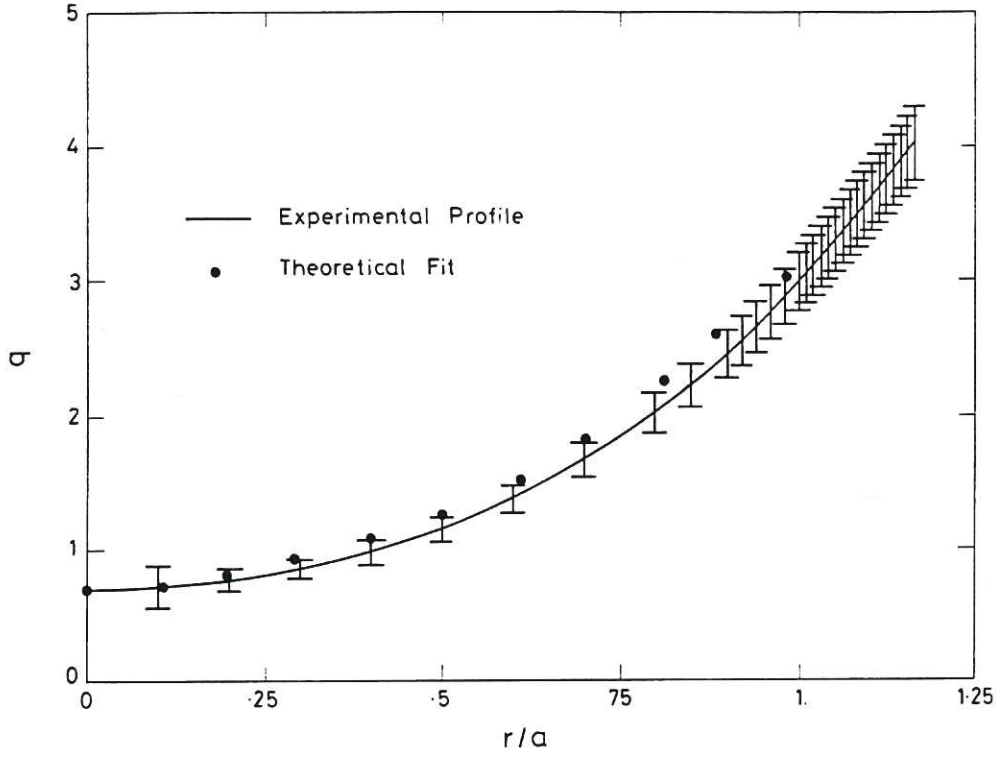

Fig. 1 Comparison between the experimentally measured $q_o(r)$ profile and the assumed theoretical fit: $q_o(r) \equiv 0.8 + 2.2\left(\frac{r}{a}\right)^2$.

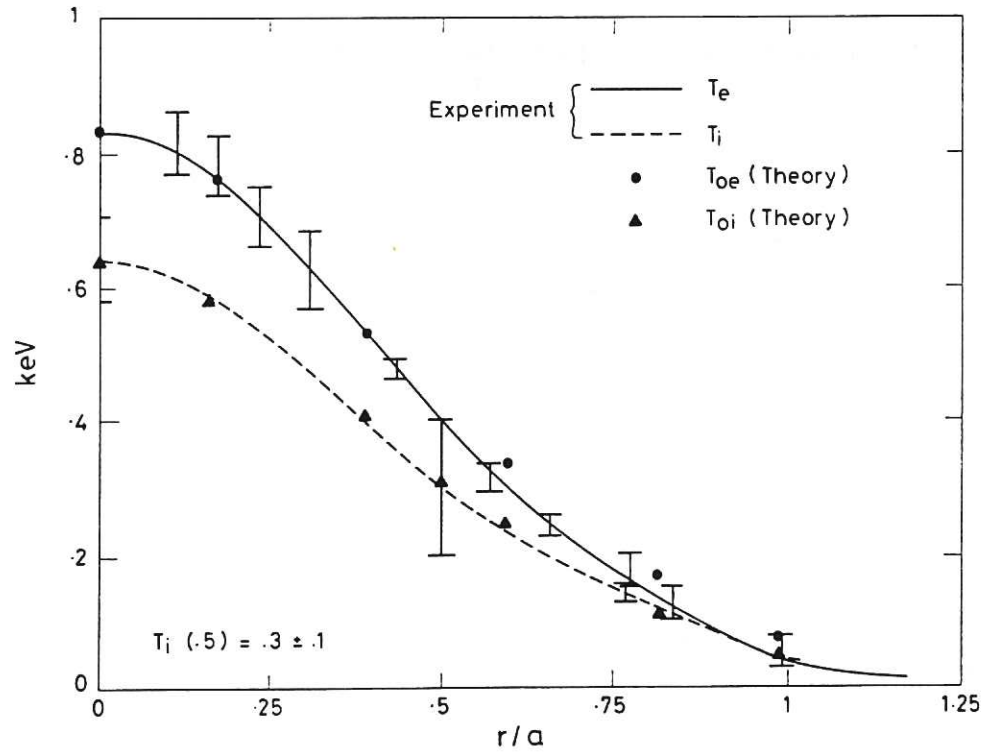

Fig. 2 Comparison between the experimentally measured temperature profiles and the assumed theoretical fits, $T_{oi,e} \equiv T_{oi,e}(o) \exp\left[-2.25\left(\frac{r}{a}\right)^2\right]$.

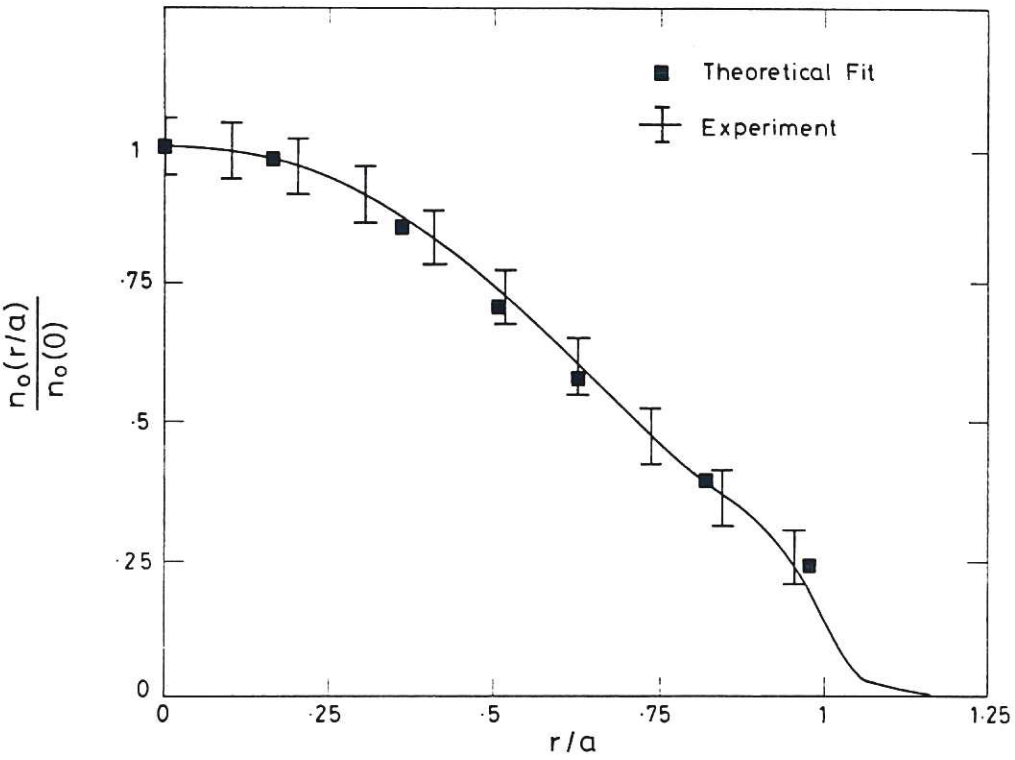

Fig. 3 Comparison between the experimentally measured electron density profile and the assumed theoretical fit: n_o (o) $(r) \equiv n_o \exp\left[-1.3\left(\frac{r}{a}\right)^2\right]$.

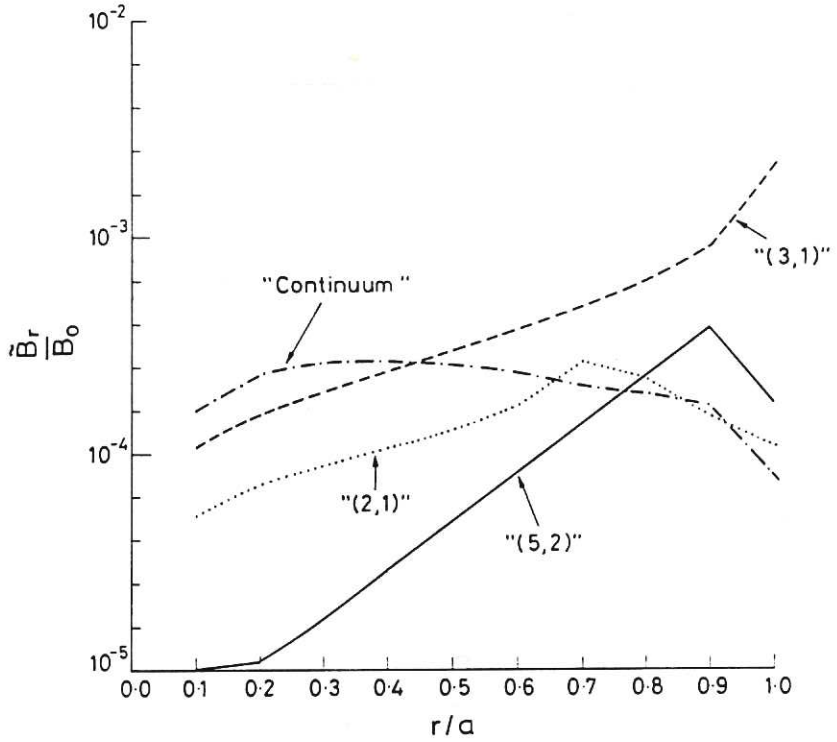

Fig. 4(a) Radial variation of the various components (c.f Eqns. (23)-(26)) of the $\frac{\tilde{B}_r}{B_o}$ spectrum assumed in the theoretical model.

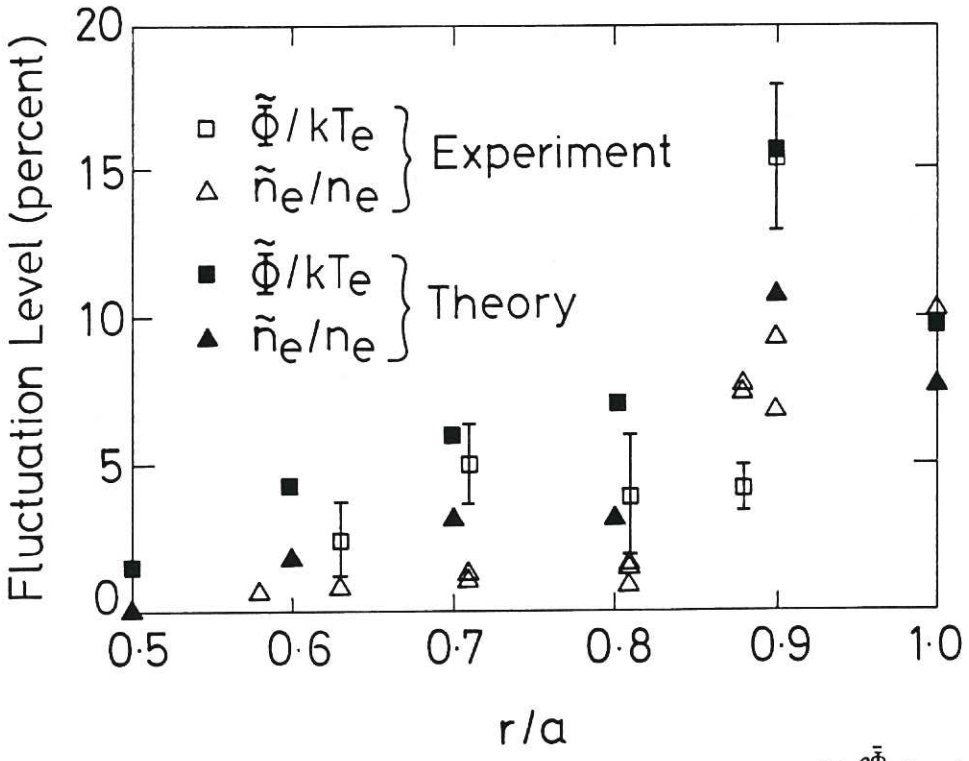

Fig. 4(b) Comparison between the experimentally measured spectra of $|\frac{e\tilde{\Phi}}{T_{oe}}|$ and $|\frac{\tilde{n}_e}{n_e}|$ at various r/a and the theoretically estimated values using the magnetic fluctuation spectrum of Fig. 4(a).

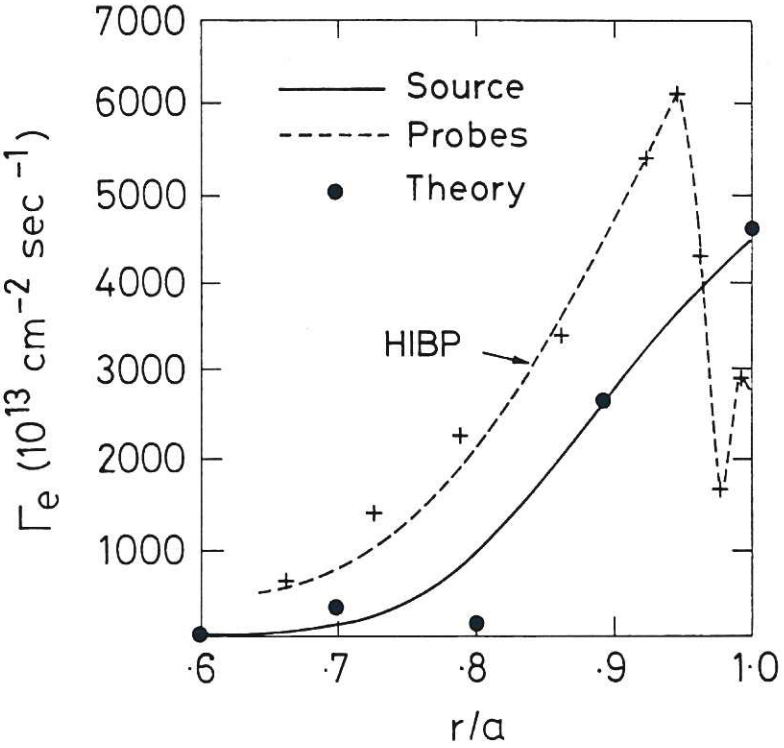

Fig. 5 Comparison between the theoretically evaluated particle flux (●) and the experimental fluxes. Experiments give fluxes obtained from particle sources and those from the HIBP measurements (the difference is attributable to experimental errors).

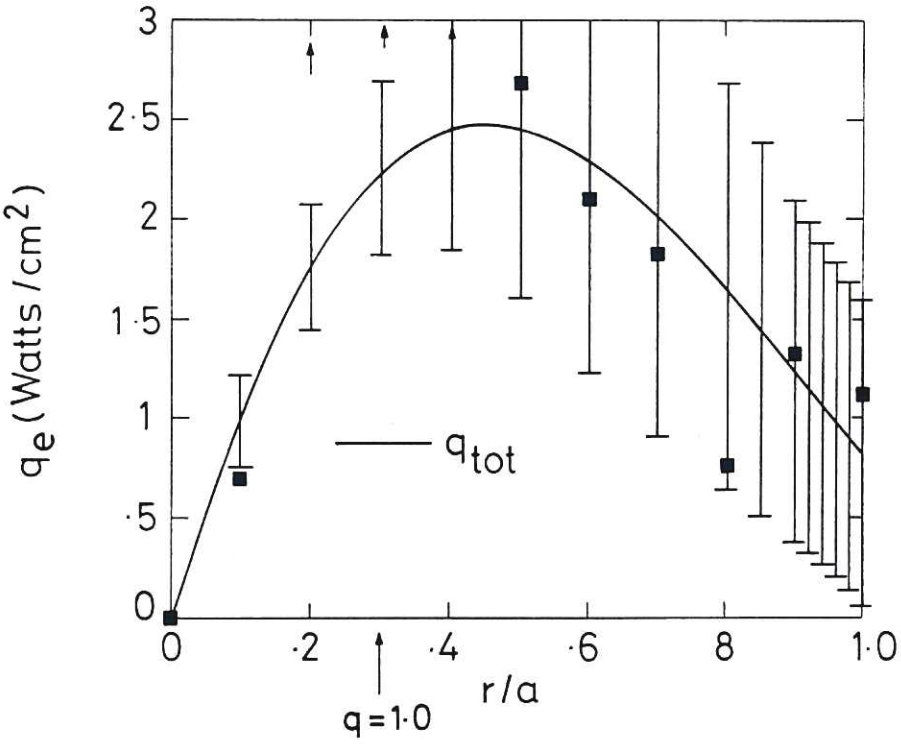

Fig. 6 Comparison between theoretically calculated electron heat flux $Q_{\perp etot}(r)$ and the total observed electron heat flux for $0 \leq r/a \leq 1$. The error bars are experimental.

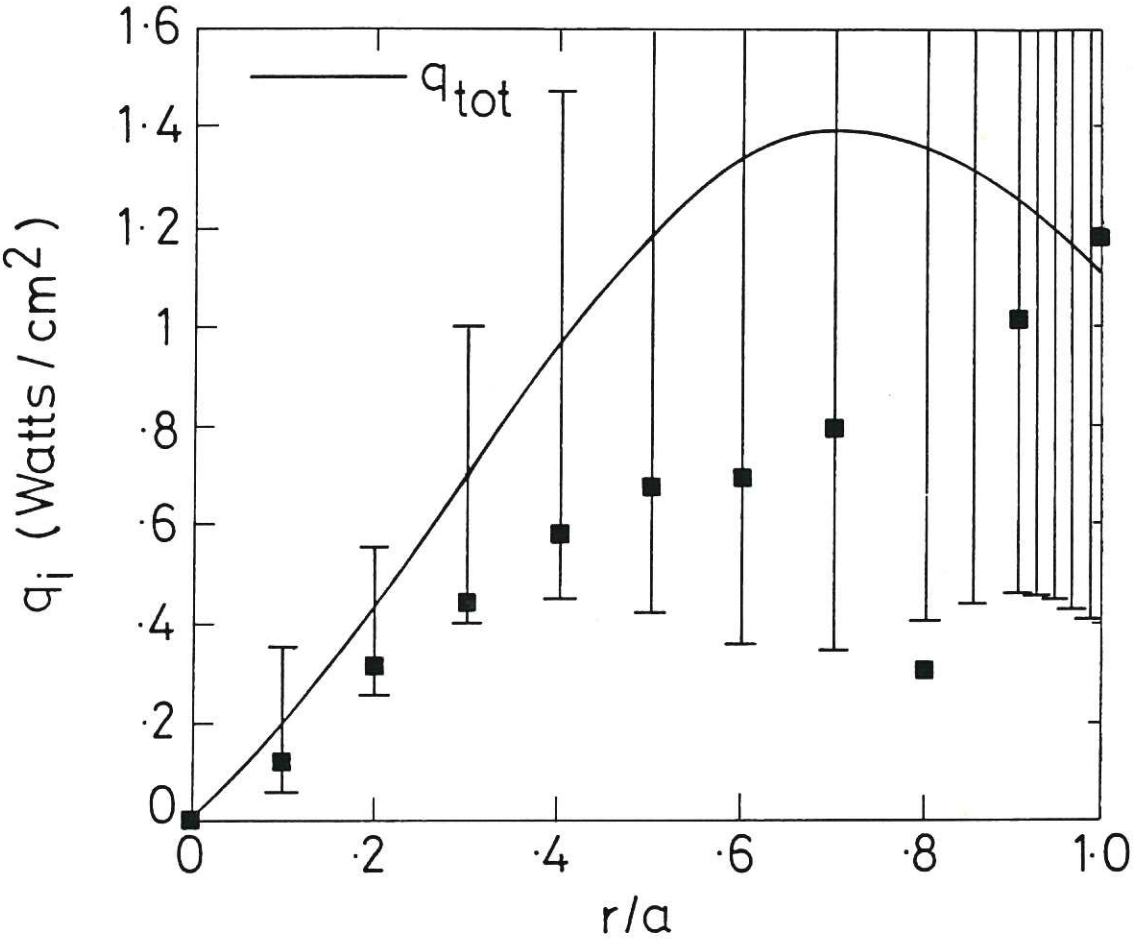

Fig. 7 Comparison between theoretical $Q_{\perp itot}(r) \equiv Q_{\perp iturb} + Q_{\perp Neo\,Class}$ and the total observed ion heat flux for $o \leq r/a \leq 1$.